Materialia 5 (2019) 100192

Contents lists available at ScienceDirect

Materialia

journal homepage: www.elsevier.com/locate/mtla

Full Length Article

Correlations between dislocation density evolution and spall strengths of Cu/Ta multilayered systems at the atomic scales: The role of spacing of KS interfaces

J. Chen[a], S.N. Mathaudhu[b], N. Thadhani[c], A.M. Dongare[a,*]

[a] Department of Materials Science and Engineering, and Institute of Materials Science, University of Connecticut, Storrs, CT 06269, United States
[b] Mechanical Engineering, and Materials Science and Engineering, University of California, Riverside, CA 92507, United States
[c] Department of Materials Science and Engineering, Georgia Institute of Technology, Atlanta, GA 30332, United States

ARTICLE INFO

Keywords:
MD simulations
Cu/Ta multilayer
KS interface
Shock compression
Spallation

ABSTRACT

The deformation and failure (spallation) behavior of Cu/Ta multilayered systems with Kurdjumov–Sachs (KS) orientation relationship is investigated at the atomic scales under shock loading conditions. Molecular dynamics (MD) simulations investigate the role of spacing between KS interfaces on the nucleation, evolution and interaction of defect structures (dislocations) in the Cu/Ta multilayered microstructures with layer thicknesses ranging from 3 nm to 47 nm. The shock compression response and failure response is investigated using the computed values of the Hugoniot elastic limit (HEL) and the spall strengths, respectively. KS interfaces serve as strong barriers to dislocation propagation and transmission across the interface and the spacing of the interfaces is observed to influence the spall behavior. The variation of the spall strength values suggests a critical interface spacing of 6 nm, below which the spall strength of the multilayered microstructure is observed to be lower than that for single-crystal Cu for the same loading conditions. The correlations between the temporal evolution of densities of various types of dislocation at the spall planes for the various microstructures and the resulting values of the spall strengths provide a clear rationale for why a microstructure results in increased/decreased spall strength values for the multiphase system.

1. Introduction

Multilayered nanocomposites are promising building blocks for next-generation materials, owing to their greatly enhanced strength, thermal stability and irradiation damage resistance in contrast to the coarse-grained microstructures [1–6]. The excellent combination of these properties for the nanocomposites is determined by distribution of bi-metal interfaces formed between the component phases in the microstructure. Both experimental and computational results have demonstrated that these bi-metal interfaces affect the plastic deformation micromechanisms of nucleation of dislocations, cross-slip across interfaces and deformation twinning that, in turn, affect the macroscopic behavior of the multilayered systems [7–11]. It is now known that the observed interface-dominated plastic deformation mechanisms are affected by the atomic structure as well as the spacing between interfaces [12–14].

More recently, substantial experimental work has investigated the modifications in the plastic deformation and failure mechanisms in these nanolayered composites under dynamic loading conditions. The differences in the elastic properties and deformation mechanisms in the component layers during shock loading can lead to substantial variations in the shock wave structure, wave reflections and interactions, and hence dynamic failure mechanisms in these composite microstructures [15,16]. The bi-metal interfaces trigger dislocation nucleation and also act as barriers to dislocation propagation under shock loading conditions, and this capability is shown to be strongly related to the atomic structure of the interface [17]. As compared to single-phase nanocrystalline metals, where grain boundaries typically act as preferential sites for voids nucleation, bi-metal interfaces do not necessarily act as weak links for void nucleation. A comparative study of the spall behavior of Cu/Ag and Cu/Nb alloys shows that voids nucleate inside Ag phase in Cu/Ag microstructures, whereas voids nucleate in the Cu regions at the Cu/Nb interfaces in Cu/Nb microstructures [18]. At large enough thicknesses of the component layers, voids are also observed to nucleate in the Cu regions away from Cu/Nb interfaces due to the interaction of reflected waves from the interfaces inside the layers [15]. Such variations of shock wave propagation, reflection and interaction behavior with varying dimensions of the component layers and interface structure can lead to significantly different spall strengths of bi-metal microstructures as compared to the pure systems. For example, spall strength values for Cu/Ag and Cu/Nb nanocrystalline alloy microstructures are found to be higher than that of the matrix Cu phase [18], whereas the spall strength of Cu/Nb multilayered system is observed to be much lower than both

* Corresponding author.
E-mail address: dongare@uconn.edu (A.M. Dongare).

https://doi.org/10.1016/j.mtla.2018.100192
Received 20 November 2018; Accepted 12 December 2018
Available online 23 December 2018

Cu and Nb component phases [15]. It is also well established that the interface spacing significantly affects the hardness and strength of multilayered systems [19–22]. This arises from the fact that, as the interface spacing decreases from hundreds of nm to a few nm, the dominant operative deformation mechanism transitions from dislocation pile-up (Hall-Petch strengthening) [23,24], to single dislocation glide (confined layer slip) [25] and furthermore to interface crossing (interface barrier strength) [26–28]. However, the time and length scale capabilities of experiments limit the investigation of the role of interface structure and spacing on the deformation and failure mechanisms under shock loading conditions.

Such insights at the atomic scales can be obtained using classical molecular dynamics (MD) simulations. MD simulations enable the investigation of the deformation and failure response of various microstructures under shock loading conditions. The deformation response can be characterized based on the computed values for the Hugoniot elastic limit (HEL) defined as the "longitudinal stress at the elastic precursor front" and the failure response is characterized based on the computed values for the spall strengths defined as the peak tensile pressures generated prior to nucleation of voids in the various microstructures. For example, MD simulations demonstrate that the HEL values are determined by the spacing of the interface that render modifications in the dislocation nucleation behavior as well as transmission behavior across multiple layers for Cu/Nb laminates [29]. The computed HEL values for Cu/Nb laminate microstructures are observed to be lower than that for single-crystal systems [30]. In addition, deformation mechanisms in Cu layers transition from homogeneous nucleation of dislocations within the layers to the nucleation at the interfaces at interface spacings lower than 20 nm, whereas deformation mechanisms in Nb layers result from homogeneous nucleation within the layers [30]. MD studies also suggest that the presence of bi-metal interfaces can shift the activation barrier for dislocation nucleation in the component layers and the barrier for dislocation transmission is observed to vary significantly with interface structure [31]. MD simulations of spall failure of Cu/Nb laminates reveal the nucleation of voids restricted to the few Cu layers near the interface, rather than at the Cu/Nb interface, suggesting that Nb plays no significant role as a stronger phase in the composite microstructure [32].

However, the fundamental understanding on the role of interfaces on the temporal evolution of defect structures, their interactions and evolution under shock loading conditions to render the variations in observed spall strength values for the multilayered microstructures is still missing. The current understanding is largely limited to the modes of deformation and the mechanisms of dislocation nucleation in multilayered FCC/BCC structures. For example, it is not clear if the trends observed in Cu/Nb multilayered microstructures (decreased spall strengths as compared to Cu) will also be observed for other FCC/BCC multilayered microstructures. In addition, a clear rationale for why a microstructure (with a structure of the FCC/BCC interface and a spacing between interfaces) results in increased/decreased spall strength values is missing. Such a rationale is crucial to tailoring and optimizing the microstructures of these materials for damage-tolerant applications.

This manuscript demonstrates a systematic study to investigate the links between interface spacing in FCC/BCC multilayered structures, the resulting variations in the temporal evolution of dislocation structures during the various stages of shock compression and spall failure and the predicted spall strength values. An exact knowledge of how the interface spacing affects the way the defect structures nucleate and evolve will enable the identification of correlations between the evolution of dislocation densities and observed macroscale dynamic response i.e. the spall strength values. This work uses the Cu/Ta multilayered system as model system to investigate these links at the atomic scales due to their unusually high hardness and yield strength (five times higher than pure Cu and Ta) as well as Hall-Petch dependence on the interface spacing under quasi-static tensile loading conditions [33]. However, it is not clear whether such ultra-high strength will be retained in these materials under dynamic loading conditions. It is also not clear if the deformation mechanisms and lower spall strengths (as compared to the component phases) observed for the multilayered Cu/Nb microstructures will also be observed in Cu/Ta multilayered microstructures. This work aims to gain a comprehensive understanding of the temporal evolution of defect density during shock wave propagation, reflections and interactions to identify the links between the interface spacing and the spall strengths for Cu/Ta multilayered systems. Lfore arge-scale MD simulations are therecarried out to investigate the effects of interface spacing using a Kurdjumov–Sachs (KS) interface structure as a model FCC/BCC interface between Cu and Ta layers. This paper is organized in the following way: the computational details are presented in Section 2. The deformation and spall behavior of Cu/Ta multilayered systems are discussed in Section 3.1, and the effects of interface spacing are discussed in Section 3.2. The correlations between defect dynamics and spall strengths are discussed in Section 3.3, followed by conclusions in Section 4.

2. Computational methods

The open source software "LAMMPS" [34] is used to carry out the MD simulations discussed here. The angular-dependent interatomic potential [35] is used to model the interactions between the atoms in the Cu/Ta system, which accurately predicts the energetics of defect structures and the Hugoniot relationships for the pure systems as well as the structural stability of the alloy system. The initial multilayered microstructures with a KS interface are created by stacking FCC Cu slabs and BCC Ta slabs with the [110] direction for Cu and the [111] direction for Ta aligned along the X direction and [112] direction for Cu and the [112] direction for Ta aligned along the Y direction, as shown schematically in Fig. 1(a). The lateral dimensions (X and Y) are determined such that the in-plane strains imposed on the component layers are minimized (< 0.1%). The dimensions of the as-created systems are 39 nm by 38 nm by 95 nm, and the total number of atoms is ~ 10 million.

The as-created multilayered microstructures are first equilibrated using Nose-Hoover isobaric-isothermal (isotropic) ensemble (NPT) at zero pressure and 300 K for 50 ps prior to shock deformation. All simulations are performed with a time step of 2 fs. An initial coherency stress is developed in the multilayered microstructure after equilibration as shown in Fig. S1 in Supplementary Note 1, and is observed to be tensile for Ta layer and compressive for Cu layer. The pressure in the system is calculated as $P = -\frac{1}{3}(\sigma_{xx} + \sigma_{yy} + \sigma_{zz})$, where σ_{xx}, σ_{yy}, and σ_{zz} are the stresses in X, Y and Z direction, respectively. The snapshots generated during simulation are divided into 100 sections along the shock direction, and physical properties such as stress and pressure are averaged over each section. The snapshots generated during the simulation are also analyzed to characterize defects (dislocations, twin faults and stacking faults, etc.) using a combination of "centro-symmetry parameter" (CSP) [36], "common neighbor analysis" (CNA) [37], "dislocation extraction algorithm" (DXA) [38,39] and "crystal analysis tool" (CAT) [40]. The characterized defects include Perfect, Shockley, Stair-rod, Frank, and Hirth and twinning partial dislocations in FCC Cu, and dislocations of Burgers vector $1/2 < 111 >$, $\langle 100 \rangle$, $\langle 110 \rangle$ in BCC Ta. More details of these methodologies can be found in [41–45]. Fig. 1(b) shows the side view of the relaxed atomic structure of the KS interface, and Fig. 1(c) shows the perpendicular view, wherein a quasi-periodic pattern formed due to intersection of intrinsic dislocation arrays can be observed [29]. These dislocation arrays can be expected to determine the deformation and spall behavior of the multilayered systems. An example initial microstructure showing the distribution of Cu/Ta KS interfaces at an interface spacing of 6 nm is shown in Fig. 2. A piston (a 3 nm thick section at the lower Z end of sample) is driven inwards at a constant velocity of 1 km/s for 10 ps to shock load the Cu/Ta microstructure. A threshold velocity of 0.9~0.95 km/s is needed to observe plastic deformation in single-crystal Cu in the [111] orientation and hence, shock velocity of 1 km/s is chosen for this study. The loading conditions of

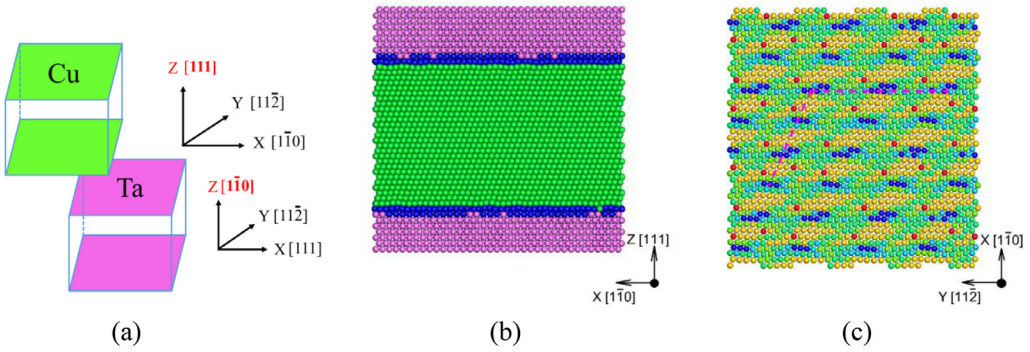

Fig. 1. (a) Schematic of the Cu/Ta stacking in a KS multilayered system. Relaxed atomic interface structures of KS interfaces: (b) side view of the interface, where atoms are colored in the following way: Cu FCC stacking (green), Ta BCC stacking (purple), and disordered Cu/Ta atoms (blue), and (c) top view of the interface atoms colored based on the Z stress component with two sets of misfit dislocation lines marked by purple dashed lines. (For interpretation of the references to colour in this figure legend, the reader is referred to the web version of this article.)

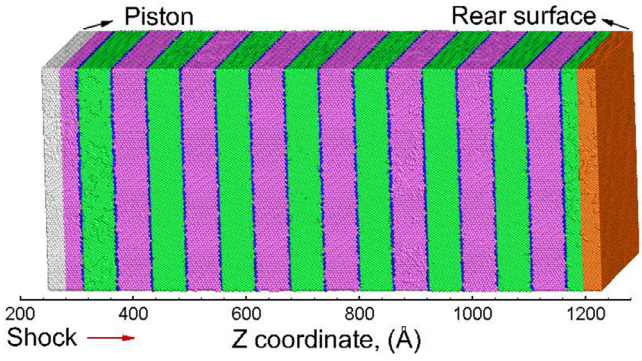

Fig. 2. Initial setup for the Ta 6 nm/Cu 6 nm multilayered system under Ta-shock loading. During the shock loading, the piston atoms (silver) are given an inward velocity (1 km/s) along positive Z direction for a duration of 10 ps, as shown by the red arrow. Atoms are colored in the following way: Cu FCC stacking (green), Cu stacking faults (red), Cu twin faults (yellow), Cu twinning partials (light blue), Cu surface (orange), Ta BCC stacking (purple), Ta twin faults (cyan), Ta surface (silver) and disordered Cu/Ta atoms (blue). (For interpretation of the references to colour in this figure legend, the reader is referred to the web version of this article.)

a constant pressure shock are used to mimic a flyer plate impact test [46], and a pulse duration is used to account for the thickness of the flyer plate before a release wave (tail of the pressure wave) is introduced in the system. The effects of interface spacing are investigated by constructing six Cu/Ta multilayered systems with an interface spacing (L) of 47 nm, 23 nm, 16 nm, 12 nm, 6 nm, and 3 nm. Periodic boundary conditions are applied in X and Y direction, and the shock (Z) direction is kept free.

3. Results and discussion

3.1. Spall behavior of Cu/Ta multilayered systems

The shock deformation and spall failure behavior of Cu/Ta multilayered systems with KS interfaces is first discussed for an interface spacing of 6 nm (as shown in Fig. 2). Since the peak shock pressures generated are determined by the interaction of the 1st layer with the piston during impact, the pressures generated by a piston impacting a Ta layer would be significantly different from the pressures generated by a piston impacting a Cu layer. Therefore, two loading scenarios are possible here: by using a piston (1st 3 nm region) to impact the 1st layers as a Ta layer (as shown in Fig. 2) or as a Cu layer, these two loading cases are referred to as "Ta-shock" and "Cu-shock", respectively. The different loading cases would result in variations in shock compression pressures and hence wave propagation behavior. Here the Cu/Ta multilayered system with an interface spacing of 6 nm for the Ta-shock loading case will be referred to as Ta 6 nm/Cu 6 nm multilayered system.

The temporal pressure evolution along the Z direction of the system is shown in Fig. 3(a) and can be used to investigate the wave propagation behavior. An initial coherency stress in the multilayered microstructure can clearly be seen in Fig. 3(a). This coherency stress results from the lattice mismatch between the component layers and is tensile for the Ta layer and compressive for the Cu layer, with a magnitude of about 0.5 GPa. The plot suggests four stages of wave propagation behavior. These stages are: "Stage 1 (SI)" comprises of shock wave loading and propagation; "Stage 2 (SII)" comprises of arrival of the tail of the shock wave as it travels towards the rear surface; "Stage 3 (SIII)" comprises of wave reflection and its interaction with the tail of the compressive wave (as indicated by the intersecting black arrows) to generate tensile pressures and nucleate voids, and "Stage 4 (SIV)" comprises of growth of voids and their coalescence to initiate failure. The evolution of overall (global) density of various types of dislocations in the Cu and Ta layers during these stages is plotted in Fig. 3(b) and 3(c), respectively. Each of these stages is discussed below for the Cu/Ta multilayered microstructures.

SI corresponds to the initiation of the compressive shock wave in the Cu/Ta microstructures. Fig. 4(a) shows the variation of the pressure along the length of the sample at intermediate times during SI. The shock velocity (U_s) calculated from the rear surface velocity profiles is 5.20 km/s for the KS (6 nm) multilayered system, which is in between the values of 6.75 km/s and 4.54 km/s observed for component phases of single crystal Cu (sc-Cu) for the [111] orientation and single crystal Ta (sc-Ta) for the [110] orientation, respectively and is much lower than their average (5.65 km/s). This suggests that the presence of KS interfaces in the multilayered microstructure serves to inhibit the propagation of the compressive waves and lower U_s. Additionally, a substantial change in the compressive pressure and particle velocity (U_p) is observed as the shockwave travels across the KS interface. Due to the different shock impedance of the two phases (as listed in Supplementary Table S1), the transmitted compressive pressure is increased as the shockwave travels from Cu to Ta layer, and decreased from Ta to Cu layer, as shown in Supplementary Fig. S2. An opposite trend is observed for U_p: increase in U_p from Ta to Cu layer, and decrease from Cu to Ta layer, as shown in Supplementary Fig. S3. This is attributed to the capability of the Ta/Cu layers to modify the pressure experienced by the following layer in the multilayered system. A more detailed discussion of the role of KS interface on the shockwave profiles, including the variation of U_p is provided in Supplementary Note 2. From Fig. 3(b) and 3(c), it can be seen that the dislocations that nucleate in the Cu layers comprise of a substantial amount of Shockley partials followed by twinning partials, whereas the dislocations in Ta layers comprise primarily

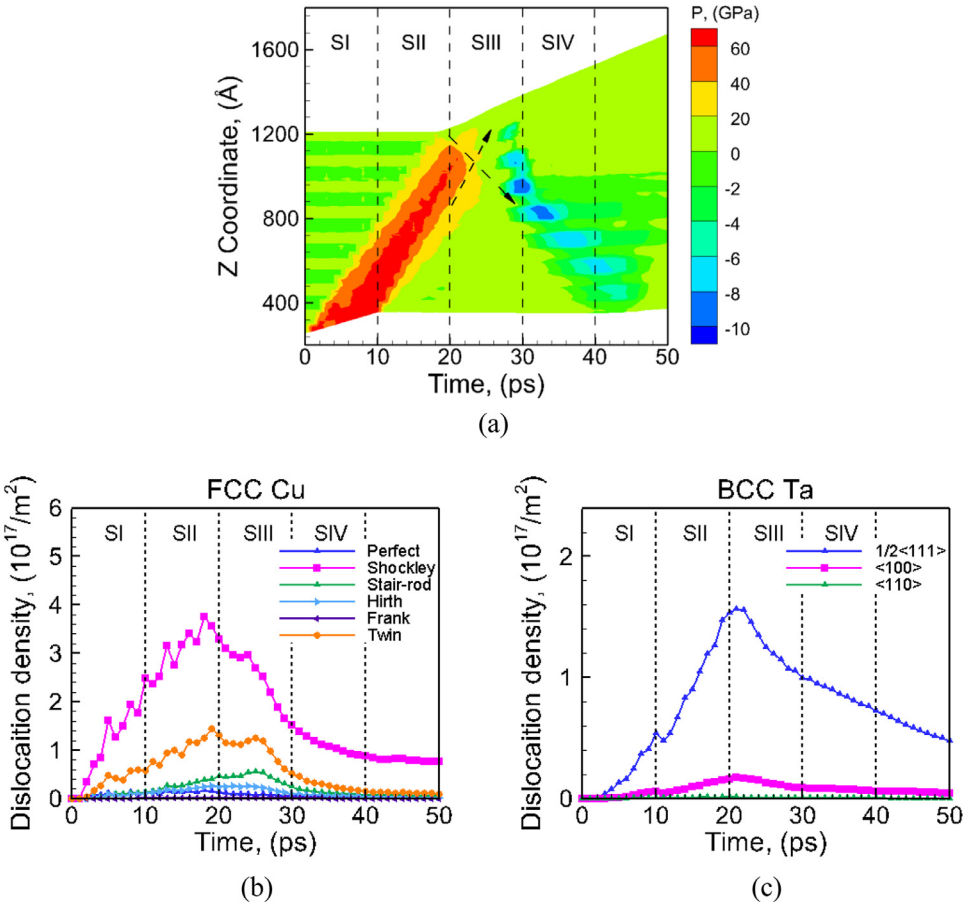

Fig. 3. (a) Evolution of pressure along the length of the Ta 6 nm/Cu 6 nm multilayered system under Ta-shock loading, evolution of dislocation densities in (b) Cu layers and (c) Ta layers.

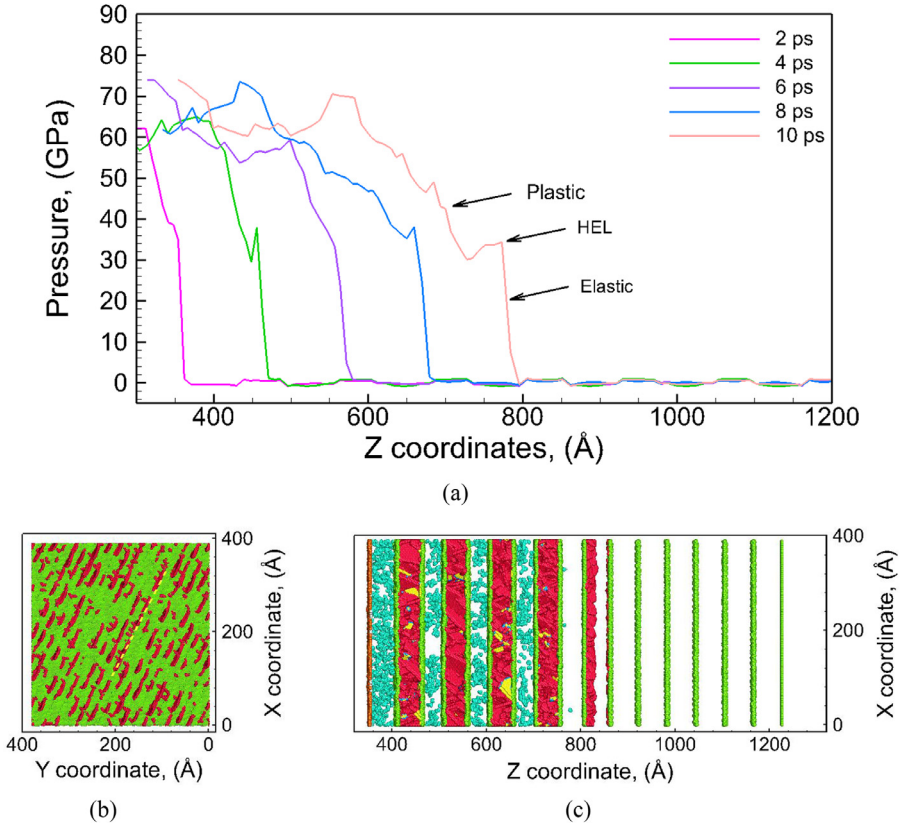

Fig. 4. (a) Shock wave profiles during SI at intermediate times for Ta 6 nm/Cu 6 nm multilayered system under Ta-shock loading, (b) Top view of the KS interface showing nucleation of stacking faults in Cu layer from the interface occurs along the misfit dislocation lines, as shown by the yellow dashed line, (c) Defect structures in the Cu and Ta layers along the length of the sample in the shock direction. The snapshot shows homogeneous nucleation of the twin faults in Ta layer (cyan atoms) as well as nucleation and propagation of stacking faults from both interfaces at the shock front towards the Cu layer. Only atoms corresponding to Cu stacking faults (red), Cu twin faults (yellow), Cu twinning partials (light blue), Cu surface (orange), Ta twin faults (cyan), Ta surface (silver) are shown here. The original Cu/Ta atoms at the interface are colored as light green. (For interpretation of the references to colour in this figure legend, the reader is referred to the web version of this article.)

of dislocations of Burgers vector $1/2 < 111 >$. Additionally, the densities of these dislocations show various drops in Cu layers as the shock wave arrives at the multiple Cu/Ta interfaces in the microstructure.

SII starts at the release of the shock pulse and ends at the arrival of the shock front at the rear surface to start the unloading process as observed in Fig. 3(a). While this release wave is able to relax the material behind the shock front to zero pressures, no change is observed in the rates of dislocation nucleation during SII. New dislocations continue to nucleate in the Cu and Ta layers as the compressive wave travels to the rear surface, as indicated in Fig. 3(b) and 3(c). For a closer look at the defect evolution during SII, defect structures (stacking faults and twin faults in Cu as shown by red and yellow atoms, respectively as well as twin faults in Ta as shown by cyan atoms) at the shock front along the length of the sample at a time of 11.6 ps are shown in Fig. 4(b) and 4(c). The plot in Fig. 4(b) shows the top view of the defects in Cu layer at the shock front. The misfit dislocation lines are marked by dashed yellow lines, and are also indicated in Fig. 1(c). The stacking faults in Cu layer can be observed to nucleate along the misfit dislocation lines at the interface and propagate into the Cu layer. The plot in Fig. 4(c) shows the side view of the defect structures along the length of the sample. The stacking faults and twin faults in Cu layers nucleate from the Cu/Ta interfaces due to the interaction of the elastic wave and propagate into the Cu layer interior. However, twin faults in Ta layers are observed to nucleate at the shock front in regions next to the Cu/Ta interface as well as in the Ta layer interior as shown by cyan atoms in Fig. 4(c). It should be noted that the characterization of dislocations in BCC using DXA is limited to ⟨100⟩, ⟨111⟩ and 'other' type of dislocations. Given that the total dislocation density is on the order if $10^{17}/m^2$, the contribution from 'others' is negligible and not considered here. While the snapshots show twinning in Ta layers, the analysis does not show any detection of 1/6 ⟨111⟩ dislocations that is indicative of twinning [47] and is likely due to the challenges in the creation of the burgers circuit for a twinning dislocation [48]. This is discussed in more detail in Supplementary Note 3. A similar preferential activation of slip systems in FCC phase from the interface that are oriented along the misfit dislocation lines, and the homogeneous nucleation of dislocations within BCC phase have also been reported for Cu/Nb multilayered system [29,49]. While defects are nucleated in both the Cu and Ta layers, no geometric alignment of the twinning planes in Ta layers and stacking faults and twin faults in Cu layers is observed here. Therefore, the KS interfaces serve as

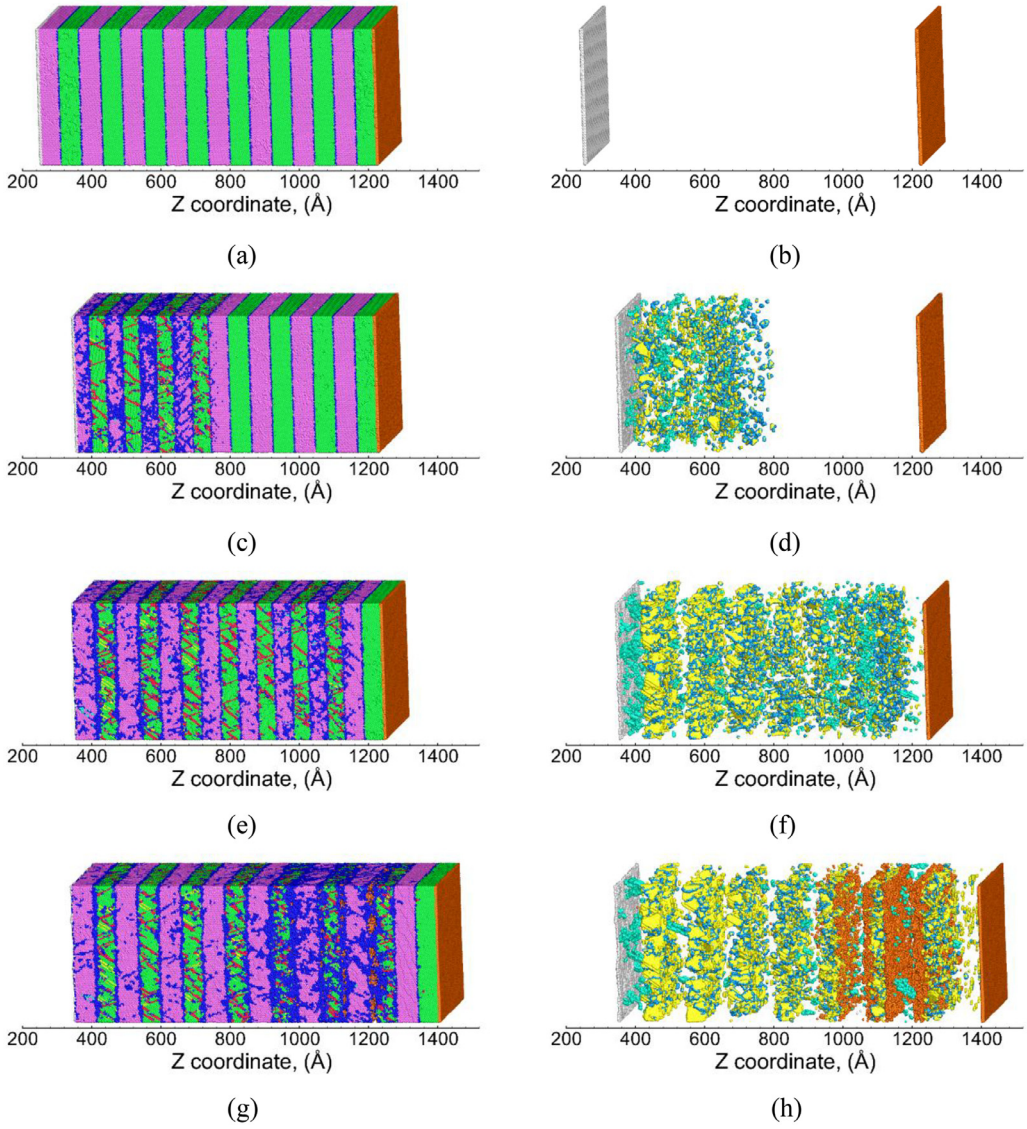

Fig. 5. Snapshots showing microstructure evolution of Ta 6 nm/Cu 6 nm multilayered system under Ta-shock loading at various stages: (a), (b) 0 ps, (c), (d) 10 ps, (e), (f) 20 ps and (g), (h) 30 ps. Left panels show the entire microstructure, and right panels show the distribution of defects (Cu twin faults, Cu twinning partials, and Ta twin faults) and damage (Cu surfaces and Ta surfaces). Atoms are colored as described in Fig. 2.

a strong barrier to dislocation transmission in Cu/Ta system in contrast to that observed for the Cu/Nb system. This high resistance to dislocation transmission has also been reported for Cu/Ta multilayered system under uniaxial tension [50] and Cu/Nb systems under indentation test [51].

The acceleration of the rear surface due to the arrival of the compressive shock wave reaching results in the onset of SIII. HEL values (using rear surface velocity profiles) during SIII of shock loading are calculated to be 37.98 GPa for the Ta 6 nm/Cu 6 nm multilayered system, which is much lower than values of that of 58.17 GPa and 51.44 GPa for the sc-Cu [111] and sc-Ta [110] system, respectively. Such lowering of HEL for the multilayered system as compared to single-crystal systems has also been reported for the Cu/Nb systems [30]. The acceleration of the rear surface results in the reflection of the shock wave, which interacts with the tail of the compressive wave to generate a state of triaxial tensile stress and lead to the nucleation of voids. The maximum tensile pressure generated in the microstructure during void nucleation is computed as the spall strength of the system. The calculated spall strength of the Ta 6 nm/Cu 6 nm multilayered system is 10.14 GPa, which is very close to sc-Cu [111] (10.06 GPa) and much lower than sc-Ta [110] (19.48 GPa). Therefore, despite the above modifications in the wave propagation behavior induced by the KS interface, the spall failure is dominated by the weaker Cu phase.

Illustrative snapshots for the Ta 6 nm/Cu 6 nm multilayered system showing defect nucleation and evolution during the various stages of shock compression and spall failure are plotted in Fig. 5. These snapshots at times of 10 ps and 20 ps (SI and SII) show a substantial amounts of stacking faults and twin faults in the Cu layers, and twin faults in Ta layers. The stacking faults and twin faults in Cu layers can be observed to extend across the entire layer, whereas the twin faults in Ta layers appear in much smaller fragments. Fig. 5(g) shows the spall failure of the multilayered microstructure as indicated by nucleation of voids in the multiple Cu layers (as shown by orange atoms) close to the Cu/Ta interfaces. However, very few voids are observed in the interior of Cu layers, and no voids are observed in Ta layers. Therefore, it is likely that the presence of interfaces weakens the few Cu atomic layers next to the interface that render weak sites for preferential void nucleation. This behavior is validated by the lowered work of separation in the Cu layers near the Cu/Ta interface based on DFT calculations [52]. Similar results have also been observed for Cu/Nb multilayered microstructures [32].

Finally, the microstructures are also characterized to identify the distribution of voids at times corresponding to peak tensile pressures. To identify voids, the simulation cell is divided into a 3-dimensional grid of cubic cells (with the same size as a Cu unit cell), and empty cells (which contains no atom) are identified. A void is defined as a cluster of two or more continuous empty cells. More details of the methodology can be found in [53]. The distribution of number of voids along the length of the sample at the time of peak tensile pressure in Cu layers is shown in Fig. 6. Here, the rectangles represent the regions where nucleation of voids occurs under the triaxial tensile stresses and are defined as the "spall plane".

3.2. Effects of spacing of KS interfaces on spall failure

The effects of interface spacing are investigated by constructing six Cu/Ta multilayered systems with an interface spacing (L) of 47 nm, 23 nm, 16 nm, 12 nm, 6 nm, and 3 nm. The Ta-shock loading case is first discussed here. Fig. 7 shows the variation of HEL for these KS multilayered systems as a function of interface spacing, in comparison with sc-Cu [111] and sc-Ta [110] system with no initial defects. The calculated HEL values are observed to decrease smoothly with decreasing interface spacing. This variation in HEL with interface spacing is different from the reported results for Cu/Nb multilayered system in [29], where a critical interface spacing of 5 nm results in a peak HEL value. However, the results show no direct trend for the variation of HEL (as plotted in Supplementary Fig. S4(a)) and spall strength (as plotted in Supplementary Fig. S4(b)) with strain rate, and therefore no correlation between strain rate and HEL or spall strength can be made here. This is attributed to the similar strain rates observed for all the multilayered systems. A more detailed discussion (along with variations) is provided in Supplementary Note 4.

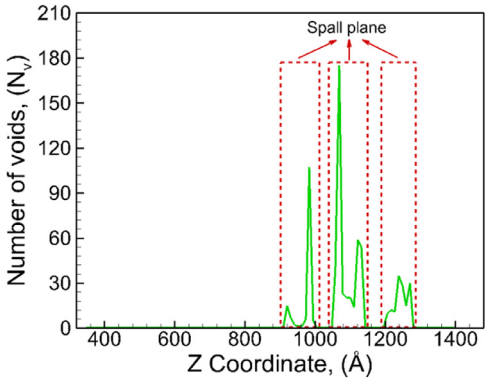

Fig. 6. Distribution of number of voids along system length in the shock direction for Ta 6 nm/Cu 6 nm multilayered system under Ta-shock loading at the time corresponding to the maximum tensile pressure. The red rectangles represent regions where voids are nucleated and are defined as the spall plane.

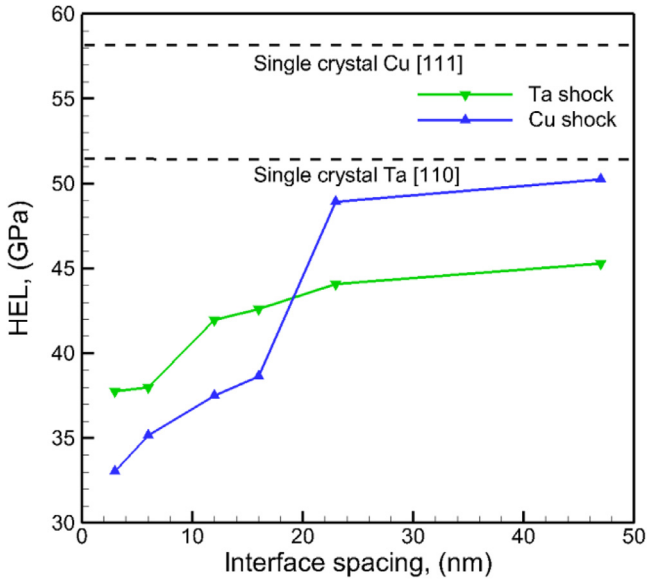

Fig. 7. Variation of HEL for KS multilayered system with interface spacing, for both Ta-shock loading and Cu-shock loading cases, as compared to the single-crystal (SC) Cu [111] and Ta [110] system.

Contour plots of the pressure evolution in the system for the various microstructures are shown in Fig. 8. No substantial changes in the compressive wave (red) propagation are observed in SI and SII from these plots. However, as the interface spacing decreases, more localized tensile regions (blue) are observed during SIII and SIV of spall failure. The tensile regions during SIV show substantial variations in tensile pressures across the layers, i.e., higher tensile pressures for the Cu layer (blue) as compared to that for the Ta layer (light blue). This variation in tensile pressure is attributed to the variations in tensile pressure generated for the same wave velocities experienced by Cu and Ta. In contrast to single-phase materials, where tensile pressures are typically generated due to interaction of rarefaction wave from the rear surface with the tail of the compression wave, the presence of Cu/Ta interfaces in the multilayered microstructure results in additional wave reflections at the interfaces that interact with the tail of the shock wave to create

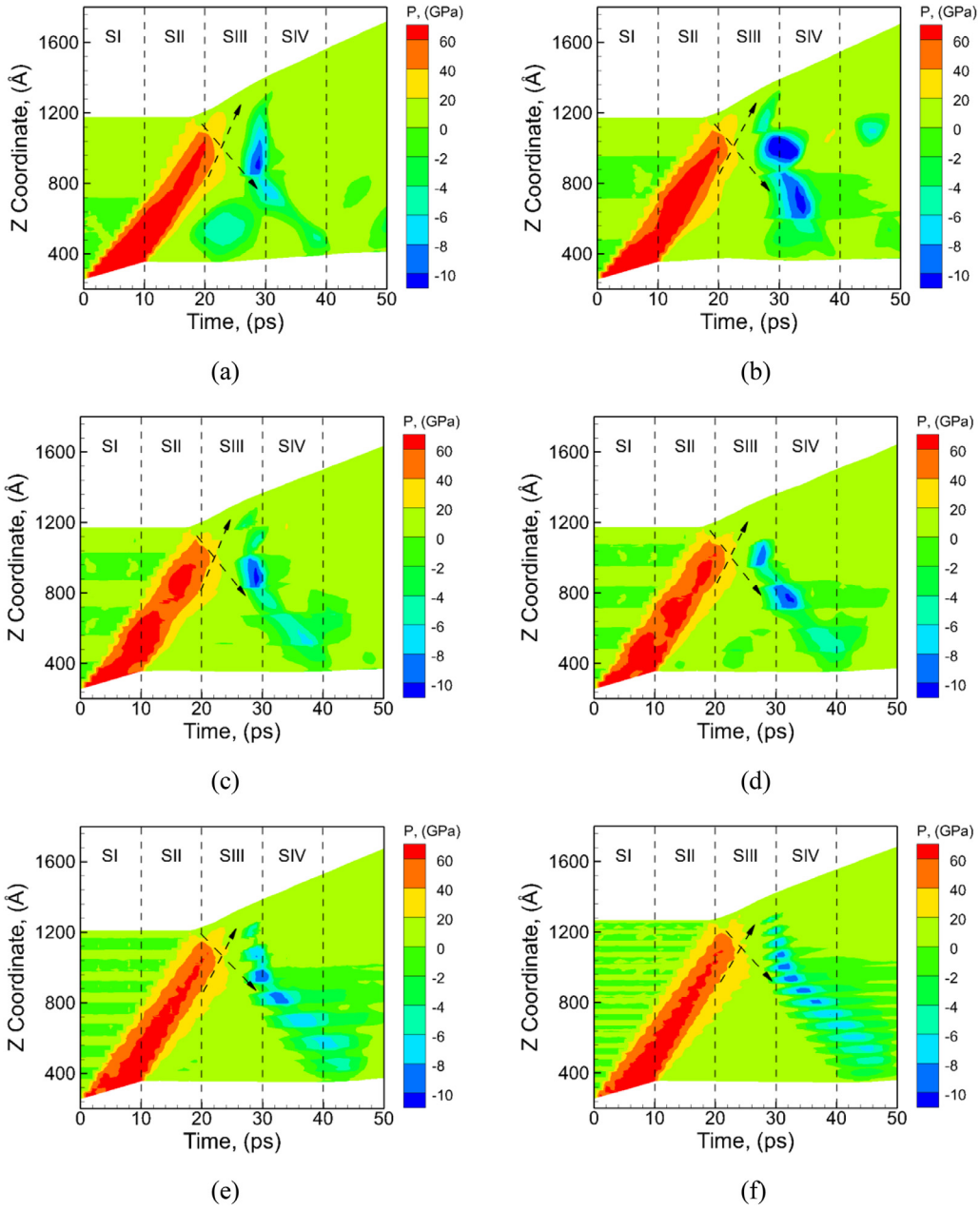

Fig. 8. Temporal evolution of pressure along the length in KS multilayered system under Ta-shock loading: (a) Ta 47 nm/Cu 47 nm, (b) Ta 23 nm/Cu 23 nm, (c) Ta 16 nm/Cu 16 nm, (d) Ta 12 nm/Cu 12 nm, (e) Ta 6 nm/Cu 6 nm, (f) Ta 3 nm/Cu 3 nm.

local tensile regions in the microstructure. The calculated peak compressive and tensile pressures and shock velocities for all the multilayered microstructures are tabulated in Table 1, in comparison with that of sc-Cu [111] and sc-Ta [110] system. The peak compressive pressures generated for the KS multilayered systems are observed to be in between that of the sc-Cu [111] and sc-Ta [110] system. The peak compressive pressures in both Cu and Ta layers are observed to be highest for an interface spacing of 23 nm among all the systems considered. The peak tensile pressures in Cu layers for the KS multilayered systems are greater than that of sc-Cu [111] system. Thus, the increased spall strength values in the presence of KS interfaces at an interface spacing greater than 3 nm may be attributed to increased shock pressures generated in the Cu layers as compared to that in sc-Cu [111] system.

To examine the spall behavior of the KS multilayered system, the snapshots of the microstructure and the corresponding defect distributions at the time of peak tensile pressure are shown in Fig. 9. For an interface spacing of 12 nm and greater (Fig. 9(a)–9(h)), a dense dislocation forest nucleated from both interfaces can be observed in the Cu layer, and voids are observed to nucleate both in the interior of the Cu layers and the Cu side of the Cu/Ta interfaces. The void nucleation in the interior of the Cu layers is due to the intense dislocation interaction at the interior, and the void nucleation at the Cu/Ta interface is due to the weak nature of the interface. However, for an interface spacing of 6 nm (Fig. 9(i) and 9(j)), void nucleation is mostly localized at the Cu side of the Cu/Ta interfaces. At this smaller interface spacing, fewer dislocations can be nucleated at the Cu layer and thus limited dislocation interaction can be observed, therefore void nucleation occurs preferentially at the interface. As the interface spacing is further reduced to 3 nm (Fig. 9(k) and 9(l)), it can be seen that the density of dislocations nucleated in the Cu layers is further reduced, and the void nucleation is observed to occur across the entire Cu layers. This is due to the small interface spacing, and the entire Cu layers can be considered

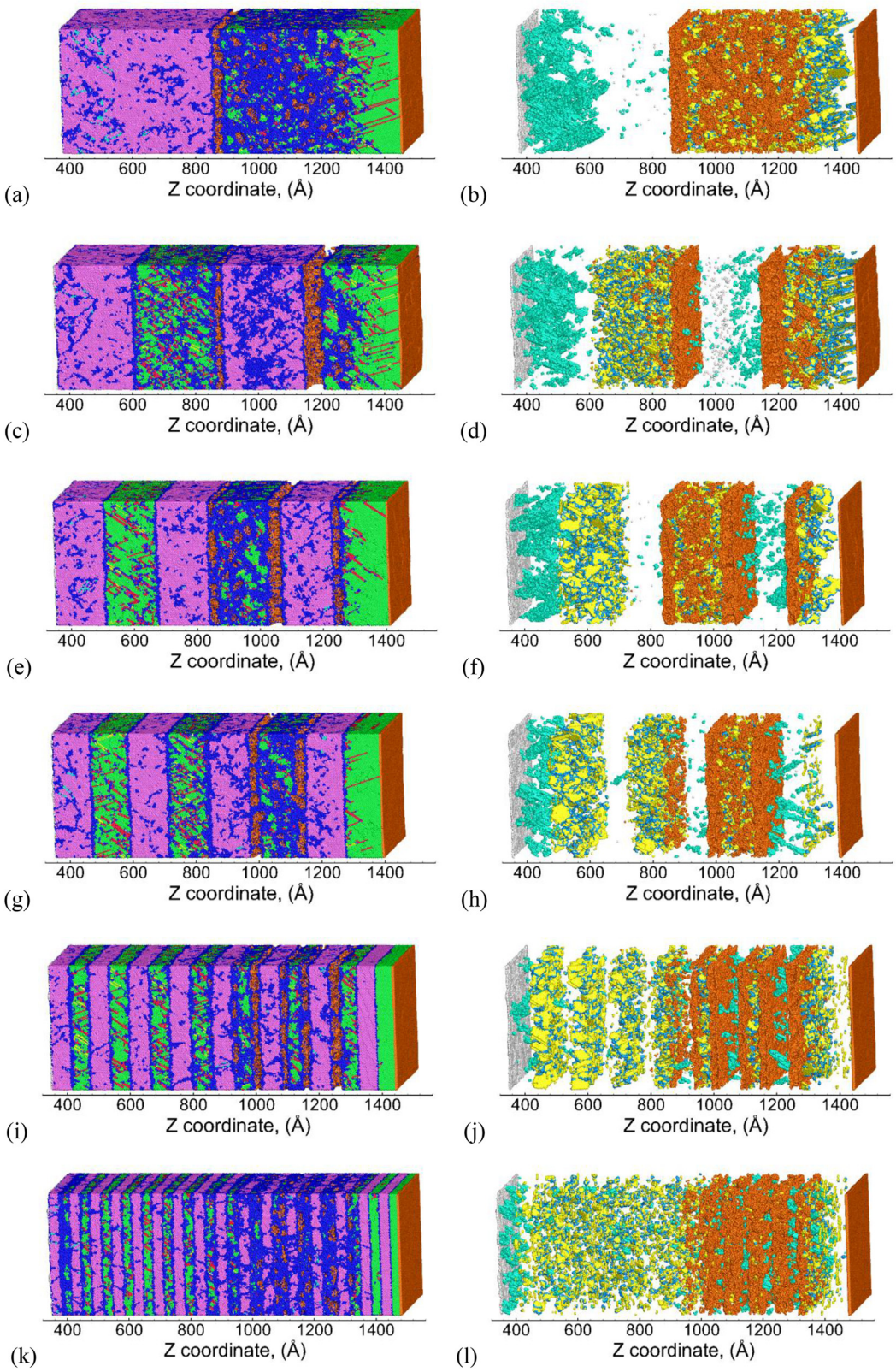

Fig. 9. Snapshots of KS multilayered system under Ta-shock loading at a time corresponding to peak tensile pressure: (a)-(b) Ta 47 nm/Cu 47 nm, (c)-(d) Ta 23 nm/Cu 23 nm, (e)-(f) Ta 16 nm/Cu 16 nm, (g)-(h) Ta 12 nm/Cu 12 nm, (i)-(j) Ta 6 nm/Cu 6 nm, (k)-(l) Ta 3 nm/Cu 3 nm. Left panels show the entire microstructure, and right panels show the distribution of defects (Cu twin faults, Cu twinning partials, and Ta twin faults) and damage (Cu surfaces and Ta surfaces). Atoms are colored as described in Fig. 2.

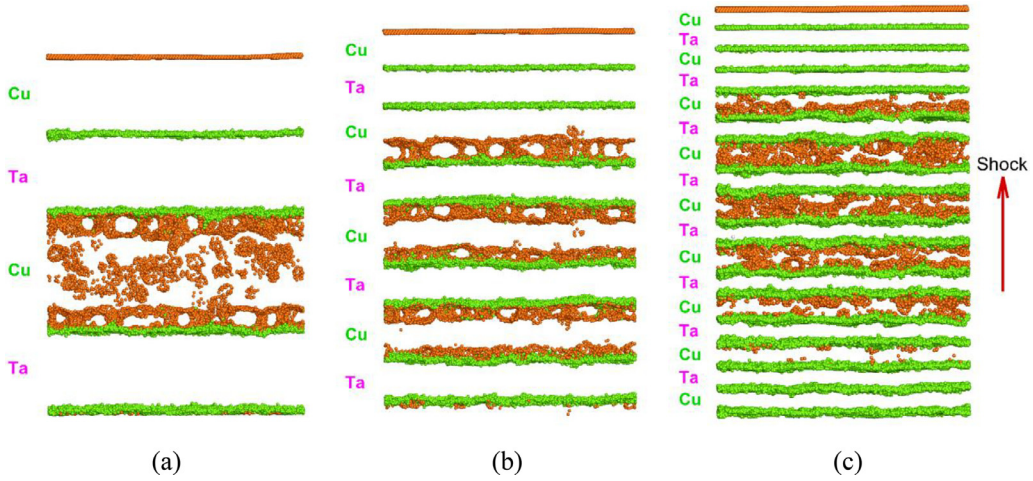

Fig. 10. Snapshots showing distribution of voids in KS multilayered system under Ta-shock loading at a time corresponding to peak tensile pressure: (a) Ta 12 nm/Cu 12 nm, (b) Ta 6 nm/Cu 6 nm, (c) Ta 3 nm/Cu 3 nm. Top half (Z coordinates > 800 Å) of the system which contains the spalled region is shown. Only atoms corresponding to Cu surface (orange), Ta surface (silver) and Cu/Ta interfaces (light green) are shown here. (For interpretation of the references to colour in this figure legend, the reader is referred to the web version of this article.)

Table 1
Peak compressive pressure ($P_{c\text{-}Cu}$, $P_{c\text{-}Ta}$), peak tensile pressure (σ_{spall}, $P_{t\text{-}Ta}$), and shock velocity (U_s) of the KS multilayered systems with varying interface spacing (L) under Ta-shock loading, as compared to sc-Cu [111] and sc-Ta [110] system. The spall strength σ_{spall} is calculated as the peak tensile pressure in Cu layers.

L (nm)	$P_{c\text{-}Cu}$ (GPa)	$P_{c\text{-}Ta}$ (GPa)	σ_{spall} (GPa)	$P_{t\text{-}Ta}$ (GPa)	Us (km/s)
47	63.18	78.88	10.80	7.42	5.22
23	72.52	79.38	10.70	14.17	5.22
16	70.69	78.50	10.73	9.85	5.21
12	68.66	75.70	10.45	6.69	5.22
6	68.01	74.06	10.14	7.92	5.20
3	66.71	73.70	9.47	8.25	5.28
sc-Cu [111]	44.70	N/A	10.06	N/A	6.75
sc-Ta [110]	N/A	78.53	N/A	19.48	4.54

to be next to the interface and therefore weakened by the interface, leading to the void nucleation and the failure of the entire Cu layers. Therefore, 3 representative failure modes are observed for the KS multilayered systems, as shown in Fig. 10. Mode 1 as shown in Fig. 10(a), is characterized by both bulk and interface failure and occurs at an interface spacing of 12 nm, and this is also the case for an interface spacing greater than 12 nm (as shown in Supplementary Fig. S6); Mode 2 as shown in Fig. 10(b), is characterized by interface dominated failure and occurs at an interface spacing of 6 nm; Mode 3 as shown in Fig. 10(c), is characterized by failure of entire Cu layers, and occurs at an interface spacing of 3 nm. Since void nucleation and failure occur only in the Cu layers for all the interface spacing considered, the spall strength of the multilayered system is therefore equal to the peak tensile pressures generated in the Cu layers. Therefore, at a small interface spacing, the spallation and failure behavior of the KS multilayered systems is dominated by the Cu/Ta interface, resulting in lower spall strengths for an interface spacing of 6 nm and 3 nm, despite the increased compressive pressure in the microstructure. These distinct deformation and failure modes demonstrate the critical role of the layer thickness in tailoring the failure behavior and the resulting spall resistance of the multilayered system.

To furthermore understand the effects of interface spacing, the temporal evolution of the overall (global) densities of various types of dislocations in the Cu layers (Perfect, Shockley, Stair-rod, Hirth, Frank and twinning partials) and in the Ta layers (Burgers vectors of $1/2<111>$, $\langle 100\rangle$ and $<110>$) are plotted in Fig. 11. No pre-existing dislocations of the above types are observed for all the multilayered microstructures considered. The variation of dislocation densities in the Cu layers during SI and SII shows various peaks that are attributed to nucleation of new dislocations as the shock wave travels in Cu layers. The various sharp dips in the dislocation density variation are attributed to the annihilation of the Cu dislocations at the Cu/Ta interfaces. The dislocation density variation for Ta layers shows a comparatively smoother increase during SI and SII. The values of dislocation density at the time of peak tensile pressure (~ 30 ps) are tabulated in Table 2 to understand the links between the spall strengths and the dislocation densities in the microstructure at the peak tensile pressures. A peak in the dislocation density of Cu is observed for an interface spacing of 23 nm and this value of the dislocation density in Cu is observed to be greater than that observed for sc-Cu [111]. Similarly, the dislocation densities in Ta layers are found to be higher than that for the sc-Ta [110] system, especially at an interface spacing greater than 6 nm. Thus, the variation of the spall strength of Cu/Ta multilayered microstructures can be correlated to the dislocation densities (Shockley partials and twinning partials). A higher twinning dislocation density in the microstructure results in higher spall strength for KS multilayered Cu/Ta microstructures as observed for nanocrystalline Cu microstructures [41]. In addition, it is noted that the highest compressive pressures are observed for an interface spacing of 23 nm for the KS interfaces and render the highest values of Shockley partial and twinning partial density. However, over the range of interface spacing considered here, no direct correlation can be identified between the dislocation density variation of the Cu/Ta microstructures and the peak shock pressures generated during shock loading, as shown in Supplementary Fig. S5. This is discussed in more detail in Supplementary Note 5.

Contour plots of the pressure evolution for Cu-shock loading are shown in Fig. 12. As observed before, localization of tensile region is observed at smaller interface spacing. The calculated peak compressive and tensile pressures and shock velocities are tabulated in Table 3. Spall strengths predicted for Cu-shock loading follows the same trend as observed for the Ta-shock loading case for interface spacing of 23 nm and lower. This value is observed to be the highest at an interface spacing of 23 nm (11.05 GPa) and 1 GPa higher than that of the sc-Cu [111] system (10.06 GPa). Additionally, the difference in the calculated spall strength of the two loading cases is found to decrease as the interface spacing decreases. For the layer dimensions considered, spall is observed either in Cu or at the Cu-Ta interface for Ta-shock loading as well as for Cu-shock loading for layer thicknesses up to 23 nm. The exception is observed for

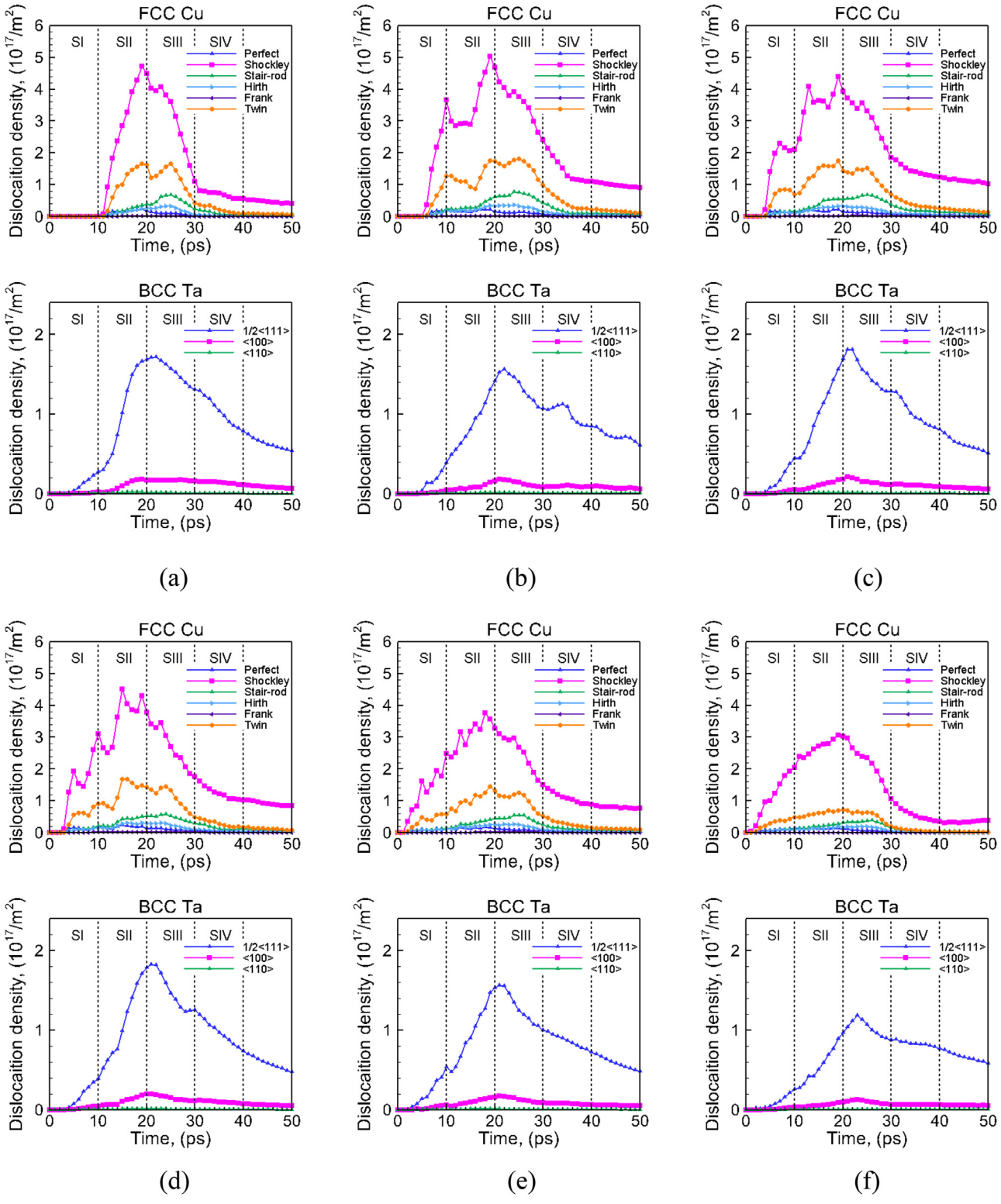

Fig. 11. Evolution of overall (global) density of various dislocations of KS multilayered system under Ta-shock loading: (a) Ta 47 nm/Cu 47 nm, (b) Ta 23 nm/Cu 23 nm, (c) Ta 16 nm/Cu 16 nm, (d) Ta 12 nm/Cu 12 nm, (e) Ta 6 nm/Cu 6 nm, (f) Ta 3 nm/Cu 3 nm. Dislocation density of Cu and Ta are shown in the top and bottom panel, respectively.

the cased of 47 nm layer thickness under Cu-shock loading wherein spall is observed in the Ta layer as well. This exception is attributed to the ratio of the layer thicknesses with the width of the shock wave generated in the system. A shock pulse of 10 ps renders a width of the shock wave of 30 - 40 nm. The width of the region that experiences triaxial tensile stresses as plotted in Fig. 6 is also observed to be 30 – 40 nm. As a result, for a bilayer system comprising of 47 nm layers, this width of the spall plane is observed to be mostly in pure Ta regions (Fig. 12(a)) for the shock pulse duration chosen, and therefore leading to spall in the Ta layer. Therefore, our results suggest a general mode of failure for the

Table 2
Global dislocation density (1017/m2) at the time of peak tensile pressure (~ 30 ps) for the KS multilayered systems with varying interface spacing (L) under Ta-shock loading, as compared to that of sc-Cu [111] and sc-Ta [110] system. The dislocations are tabulated for Perfect, Shockley, Stair-rod and twinning partials in Cu layers and dislocations of Burgers vector 1/2 < 111 >, ⟨100⟩ and ⟨110⟩ in Ta layers.

L (nm)	Dislocations in Cu layers				Dislocations in Ta layers		
	Perfect	Shockley	Stair-rod	Twin	1/2 < 111>	<100>	<110>
47	0.04	1.59	0.33	0.67	1.34	0.16	0.01
23	0.09	2.41	0.43	0.98	1.07	0.09	0.01
16	0.09	2.16	0.46	0.81	1.29	0.11	0.01
12	0.05	1.47	0.25	0.40	1.14	0.11	0.00
6	0.06	1.51	0.25	0.52	1.00	0.09	0.01
3	0.03	0.91	0.12	0.15	0.89	0.07	0.01
sc-Cu [111]	0.08	2.25	0.39	0.81	N/A	N/A	N/A
sc-Ta [110]	N/A	N/A	N/A	N/A	0.83	0.08	0.00

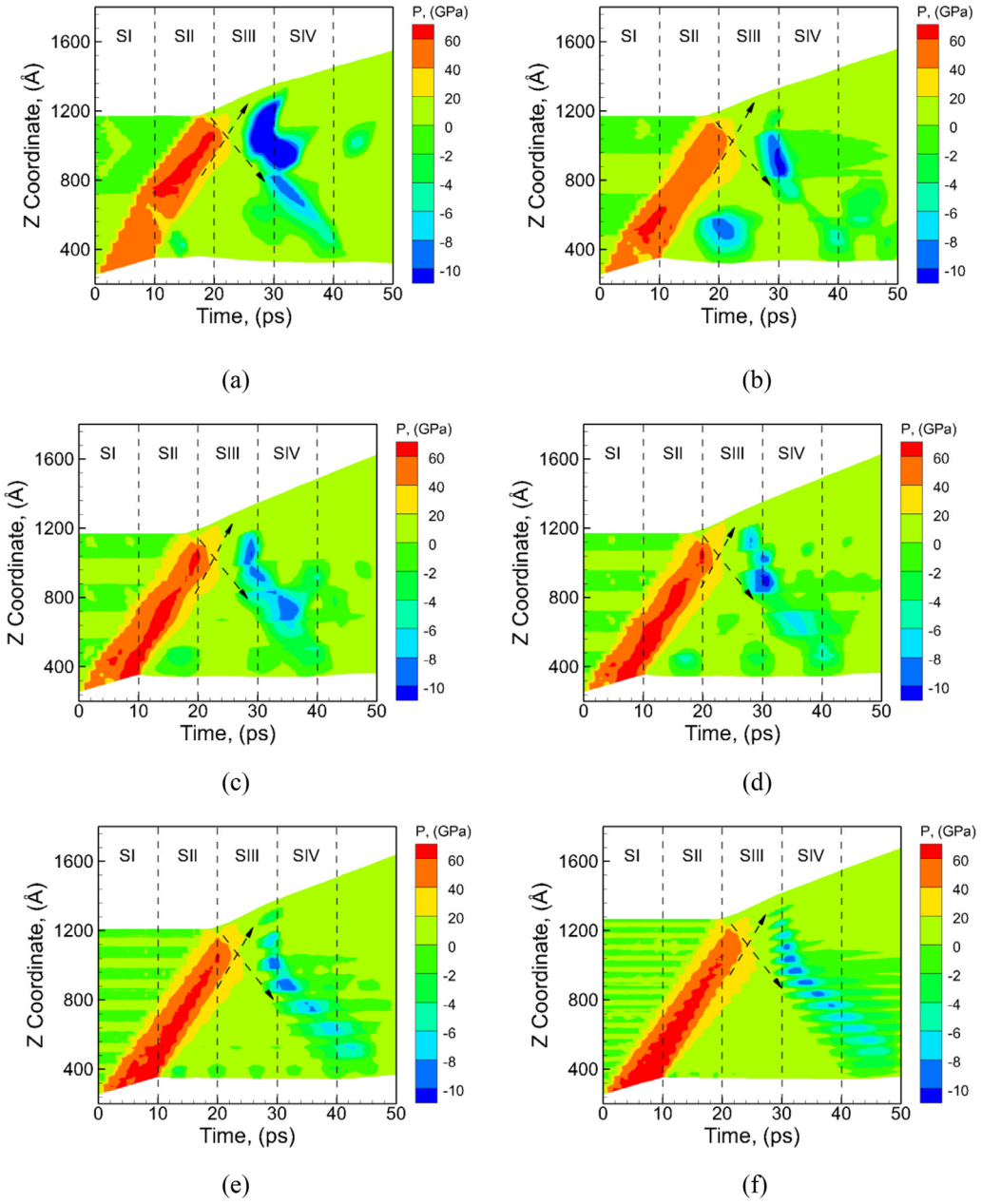

Fig. 12. Temporal evolution of pressure in the KS multilayered system under Cu-shock loading: (a) Cu 47 nm/Ta 47 nm, (b) Cu 23 nm/Ta 23 nm, (c) Cu 16 nm/Ta 16 nm, (d) Cu 12 nm/Ta 12 nm, (e) Cu 6 nm/Ta 6 nm, (f) Cu 3 nm/Ta 3 nm.

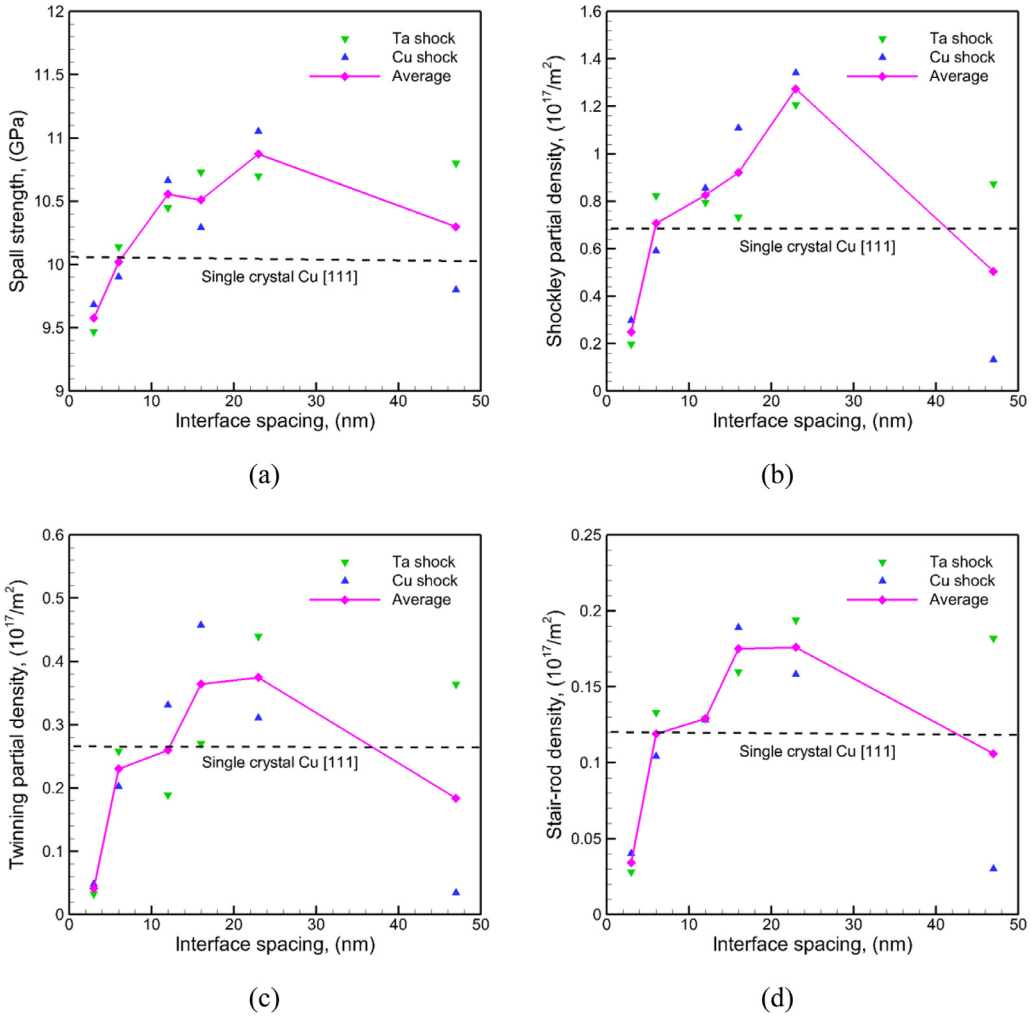

Fig. 13. Variation of (a) spall strengths in Cu layers, and densities of (b) Shockley partials, (c) twinning partials and (d) Stair-rod partials in Cu layers at the spall plane for various values of KS interface spacing in the multilayered system.

Table 3
Peak compressive pressure ($P_{c\text{-}Cu}$, $P_{c\text{-}Ta}$), peak tensile pressure (σ_{spall}, $P_{t\text{-}Ta}$), and shock velocity (U_s) of the KS multilayered systems with varying interface spacing (L) under Cu-shock loading, as compared to sc-Cu [111] and sc-Ta [110] system.

L (nm)	$P_{c\text{-}Cu}$ (GPa)	$P_{c\text{-}Ta}$ (GPa)	σ_{spall} (GPa)	$P_{t\text{-}Ta}$ (GPa)	Us (km/s)
47	60.74	65.35	9.80	18.49*	5.45
23	64.67	70.26	11.05	7.00	5.43
16	73.22	73.67	10.29	9.42	5.42
12	71.24	77.50	10.66	9.05	5.37
6	72.50	75.92	9.90	8.86	5.34
3	69.44	74.13	9.68	7.87	5.28
sc-Cu [111]	44.70	N/A	10.06	N/A	6.78
sc-Ta [110]	N/A	78.53	N/A	19.48*	4.48

* These values refer to cases where void nucleation is observed in Ta layers and are therefore a spall strength value.

multilayered system to be next to the interface at the weaker phase, as well as exception to this general observation at a larger interface spacing (47 nm) greater than the typical width of the spall plane (30–40 nm). The spall strength in the Ta layer is calculated to be 18.49 GPa, slightly lower than sc-Ta [110] (19.48 GPa). At an interface spacing of 23 nm, as shown in Fig. 12(b), local region of tensile pressure is generated in the Cu layer which results in incipient void nucleation at the Cu/Ta interface at ~ 20 ps. This local tensile wave is generated due to the interaction of the reflected wave from the 1st Cu/Ta interfaces and the tail of the compressive wave, and lasts only for a few ps and is relieved at a later stage. The incipient void nucleation due to the release waves generated at the interface has also been reported for Cu/Nb multilayer system [15]. For all the other interface spacing, voids are observed to nucleate only in the interior of the Cu layers and Cu side of the Cu/Ta interface. The snapshots of the microstructure at the time of peak tensile pressure, and the corresponding defect distributions for these cases are shown in Supplementary Fig. S7, and the void distribution is shown in Supplementary Fig. S8. The observed void nucleation behavior is found to be similar to the Ta-shock loading case, and distinctive failure modes are observed for the interface spacing of 12 nm and greater (Mode1: Supplementary Fig. S8(a)–8(d)), 6 nm (Mode 2: Supplementary Fig. S8(e)) and 3 nm (Mode 3: Supplementary Fig. S8(f)). As can be seen in Fig. 7, the variation of HEL for the Cu-shock loading case shows a more significant decrease with the decrease of interface spacing. Values of dislocation density at the time of peak tensile pressure (~ 30 ps) are tabulated in Table 4. A similar variation of the densities of all types of dislocations is observed here as compared to the Ta-shock loading conditions.

3.3. Correlations between local defect densities and spall strengths

The variation of the spall strengths of the multilayered systems is determined by the evolution of various types of dislocations in the microstructure. Therefore, it is crucial to investigate whether there exists

Table 4
Global dislocation density ($10^{17}/m^2$) at the time of peak tensile pressure (~ 30 ps) for the KS multilayered systems with varying interface spacing (L) under Cu-shock loading, as compared to that of sc-Cu [111] and sc-Ta [110] system. The dislocations are tabulated for Perfect, Shockley, Stair-rod and twinning partials in Cu layers and dislocations of Burgers vector 1/2 < 111 >, ⟨100⟩ and ⟨110⟩ in Ta layers.

L (nm)	Dislocations in Cu layers				Dislocations in Ta layers		
	Perfect	Shockley	Stair-rod	Twin	1/2 < 111>	<100>	<110>
47	0.04	1.91	0.22	0.28	0.54	0.03	0.00
23	0.11	2.33	0.27	0.55	1.04	0.09	0.00
16	0.09	2.10	0.34	0.85	1.04	0.09	0.00
12	0.06	1.59	0.24	0.63	1.01	0.09	0.00
6	0.06	1.79	0.33	0.61	0.95	0.08	0.00
3	0.03	0.88	0.11	0.15	0.85	0.07	0.01
sc-Cu [111]	0.08	2.25	0.39	0.81	N/A	N/A	N/A
sc-Ta [110]	N/A	N/A	N/A	N/A	0.83	0.08	0.00

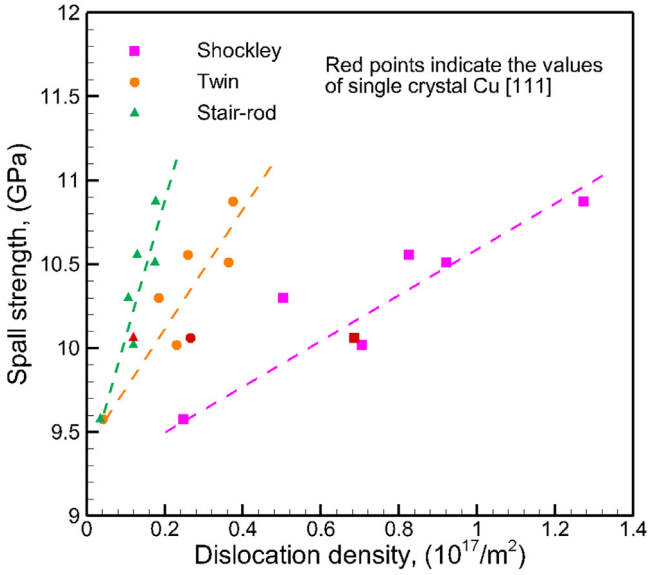

Fig. 14. Correlations of spall strengths in Cu layers with Shockley partial, twinning partial and Stair-rod dislocation densities at the spall plane in Cu layers for KS multilayered system. Here the average values of Ta-shock and Cu-shock loading cases are shown.

a strong correlation of the spall strength with the density of dislocations in the microstructure.

The variation of the spall strength values in Cu layers is plotted as a function of interface spacing in Fig. 13(a) based on values obtained for the Cu-shock and Ta-shock loading conditions, and their average values. The plot shows a clear peak in spall strength at an interface spacing of 23 nm among all the systems considered. To correlate this variation of the spall strengths with the defect densities, the variation of the densities of local Shockley partials, twinning partials and Stair-rod dislocations at the spall plane with interface spacing is plotted in Fig. 13(b), 13(c) and 13(d), respectively, at the time of peak tensile pressures. A correlation can be observed between the spall strength values and the density of Shockley partials, twinning partials and Stair-rod partials that show peak values at an interface spacing of 23 nm. This correlation is especially significant for Shockley partials and Stair-rods. For example, an interface spacing of 6 nm for the multilayered systems that renders a local average Shockley partial and Stair-rod density that is very close to the sc-Cu [111] system also renders an average spall strength that is also very close to the sc-Cu [111] system. Thus, a higher spall strength of the KS multilayered systems is likely to be determined by a higher density of local Shockley partial, twinning partial and Stair-rod density at the spall plane in the multilayered microstructure. To see this correlation more clearly, Fig. 14 shows the variation of the spall strength with local dislocation densities for the multilayered systems and sc-Cu [111] system, where only the average values of the Ta-shock and Cu-shock loading conditions are shown. A strong linear correlation can be observed for Shockley partials, twinning partials and Stair-rod dislocations from the plot.

Therefore, the variations in the spacing of the KS Cu/Ta interfaces result in variations in the evolution of defect structures that can either strengthen or weaken the multilayered microstructures, demonstrating the significant role of dislocation plasticity in determining the spall strengths of the multilayered microstructure. In comparison with previously reported spall strengths of Cu/Nb systems wherein the spall strength of Cu/Nb multilayered system is found to be lower than both Cu and Nb component phases, Cu/Ta multilayered microstructures render higher spall strengths than Cu for interface spacing greater than 6 nm. Future efforts will aim to investigate the role of other types of Cu/Ta interface structures on the deformation and spall behavior of the multilayered microstructures.

4. Conclusion

The shock loading and spall failure behavior of Cu/Ta multilayered microstructures comprising of KS interfaces is investigated at the atomic scales using MD simulations. The major findings of this work are:

1 The Cu/Ta KS interfaces can serve as sources for dislocation nucleation and strong barriers to dislocation transmission across multilayers.
2 The failure modes and spall strengths of the KS multilayered microstructures are strongly dependent upon the interface spacing, as indicated by 3 distinct failure modes at different interface spacing: i). Bulk and interface failure at an interface spacing of 12 nm and greater, ii). Interface dominated failure at an interface spacing of 6 nm, and iii). Failure of entire Cu layers at an interface spacing of 3 nm. At smaller interface spacing, the failure is dominated by Cu/Ta interface, resulting in lower spall strengths.
3 The general failure behavior of the KS multilayered system is characterized by failure in the few Cu layers (the weaker phase) next to the interface which act as weak links, and an exception to this general observation is observed at an interface spacing (47 nm) greater than the spall width (30–40 nm), where spall failure occurs inside Ta layer.
4 A direct correlation between the spall strengths and the local Shockley partial, twinning partial and Stair-rod densities at the spall plane is observed wherein peak densities of these dislocations are observed for microstructures that render peak spall strengths at an interface spacing of 23 nm. This correlation demonstrates the significant role

of dislocation plasticity in determining the spall strengths of the KS multilayered microstructure.

The Cu/Ta KS multilayered microstructures therefore show significant promise in the optimization of damage tolerant materials for applicability in dynamic loading conditions.

Acknowledgements

This material is based upon work supported by the National Science Foundation (NSF) CMMI Grant-1454547.

Declaration of interest

None

Supplementary material

Supplementary material associated with this article can be found, in the online version, at doi:doi:10.1016/j.mtla.2018.100192.

References

[1] N. Li, M. Nastasi, A. Misra, Defect structures and hardening mechanisms in high dose helium ion implanted Cu and Cu/Nb multilayer thin films, Int. J. Plast. 32-33 (Supplement C) (2012) 1–16.
[2] W. Han, M.J. Demkowicz, N.A. Mara, E. Fu, S. Sinha, A.D. Rollett, Y. Wang, J.S. Carpenter, I.J. Beyerlein, A. Misra, Design of radiation tolerant materials via interface engineering, Adv. Mater. 25 (48) (2013) 6975–6979.
[3] Y. Chen, E. Fu, K. Yu, M. Song, Y. Liu, Y. Wang, H. Wang, X. Zhang, Enhanced radiation tolerance in immiscible Cu/Fe multilayers with coherent and incoherent layer interfaces, J. Mater. Res. 30 (9) (2015) 1300–1309.
[4] M.J. Demkowicz, R.G. Hoagland, J.P. Hirth, Interface structure and radiation damage resistance in Cu-Nb multilayer nanocomposites, Phys. Rev. Lett. 100 (13) (2008) 136102.
[5] A. Misra, M.J. Demkowicz, X. Zhang, R.G. Hoagland, The radiation damage tolerance of ultra-high strength nanolayered composites, JOM 59 (9) (2007) 62–65.
[6] I.J. Beyerlein, A. Caro, M.J. Demkowicz, N.A. Mara, A. Misra, B.P. Uberuaga, Radiation damage tolerant nanomaterials, Mater. Today 16 (11) (2013) 443–449.
[7] I.J. Beyerlein, M.J. Demkowicz, A. Misra, B.P. Uberuaga, Defect-interface interactions, Prog. Mater. Sci. 74 (Supplement C) (2015) 125–210.
[8] N.A. Mara, I.J. Beyerlein, Interface-dominant multilayers fabricated by severe plastic deformation: Stability under extreme conditions, Curr. Opin. Solid State Mater. Sci. 19 (5) (2015) 265–276.
[9] S. Shao, J. Wang, Relaxation, structure, and properties of semicoherent interfaces, JOM 68 (1) (2016) 242–252.
[10] I.J. Beyerlein, J.R. Mayeur, R.J. McCabe, S.J. Zheng, J.S. Carpenter, N.A. Mara, Influence of slip and twinning on the crystallographic stability of bimetal interfaces in nanocomposites under deformation, Acta Mater. 72 (Supplement C) (2014) 137–147.
[11] I.J. Beyerlein, J. Wang, K. Kang, S.J. Zheng, N.A. Mara, Twinnability of bimetal interfaces in nanostructured composites, Mater. Res. Lett. 1 (2) (2013) 89–95.
[12] J. Wang, A. Misra, An overview of interface-dominated deformation mechanisms in metallic multilayers, Curr. Opin. Solid State Mater. Sci. 15 (1) (2011) 20–28.
[13] I.J. Beyerlein, N.A. Mara, J. Wang, J.S. Carpenter, S.J. Zheng, W.Z. Han, R.F. Zhang, K. Kang, T. Nizolek, T.M. Pollock, Structure–property–functionality of bimetal interfaces, JOM 64 (10) (2012) 1192–1207.
[14] T. Zhu, J. Li, Ultra-strength materials, Prog. Mater. Sci. 55 (7) (2010) 710–757.
[15] W.Z. Han, E.K. Cerreta, N.A. Mara, I.J. Beyerlein, J.S. Carpenter, S.J. Zheng, C.P. Trujillo, P.O. Dickerson, A. Misra, Deformation and failure of shocked bulk Cu–Nb nanolaminates, Acta Mater. 63 (Supplement C) (2014) 150–161.
[16] P.E. Specht, N.N. Thadhani, T.P. Weihs, Configurational effects on shock wave propagation in Ni-Al multilayer composites, J. Appl. Phys. 111 (7) (2012) 073527.
[17] W.Z. Han, A. Misra, N.A. Mara, T.C. Germann, J.K. Baldwin, T. Shimada, S.N. Luo, Role of interfaces in shock-induced plasticity in Cu/Nb nanolaminates, Philos. Mag. 91 (32) (2011) 4172–4185.
[18] S.J. Fensin, E.K. Walker, E.K. Cerreta, C.P. Trujillo, D.T. Martinez, G.T. Gray, Dynamic failure in two-phase materials, J. Appl. Phys. 118 (23) (2015) 235305.
[19] A. Misra, J.P. Hirth, R.G. Hoagland, Length-scale-dependent deformation mechanisms in incoherent metallic multilayered composites, Acta Mater. 53 (18) (2005) 4817–4824.
[20] K.Y. Yu, Y. Liu, S. Rios, H. Wang, X. Zhang, Strengthening mechanisms of Ag/Ni immiscible multilayers with fcc/fcc interface, Surf. Coat. Technol. 237 (Supplement C) (2013) 269–275.
[21] Y. Chen, Y. Liu, C. Sun, K.Y. Yu, M. Song, H. Wang, X. Zhang, Microstructure and strengthening mechanisms in Cu/Fe multilayers, Acta Mater. 60 (18) (2012) 6312–6321.
[22] T. Nizolek, I.J. Beyerlein, N.A. Mara, J.T. Avallone, T.M. Pollock, Tensile behavior and flow stress anisotropy of accumulative roll bonded Cu-Nb nanolaminates, Appl. Phys. Lett. 108 (5) (2016) 051903.
[23] P.M. Anderson, C. Li, Hall-Petch relations for multilayered materials, Nanostruct. Mater. 5 (3) (1995) 349–362.
[24] L.H. Friedman, D.C. Chrzan, Scaling theory of the Hall-Petch relation for multilayers, Phys. Rev. Lett. 81 (13) (1998) 2715–2718.
[25] N. Li, J. Wang, A. Misra, J.Y. Huang, Direct observations of confined layer slip in Cu/Nb multilayers, Microsc. Microanal. 18 (5) (2012) 1155–1162.
[26] J.S. Koehler, Attempt to design a strong solid, Phys. Rev. B. 2 (2) (1970) 547–551.
[27] P.M. Hazzledine, M.A. Grinfeld, S.I. Rao, Coherency and loss of coherency in multilayers, MRS Proceed. 505 (2011).
[28] V. Ramaswamy, W.D. Nix, B.M. Clemens, Coherency and surface stress effects in metal multilayers, Scripta Mater. 50 (6) (2004) 711–715.
[29] R.F. Zhang, T.C. Germann, X.Y. Liu, J. Wang, I.J. Beyerlein, Layer size effect on the shock compression behavior of fcc–bcc nanolaminates, Acta Mater. 79 (Supplement C) (2014) 74–83.
[30] R. Zhang, J. Wang, X. Liu, I.J. Beyerlein, T.C. Germann, Nonequilibrium molecular dynamics simulations of shock wave propagation in nanolayered Cu/Nb nanocomposites, AIP Conf. Proc. 1426 (1) (2012) 1251–1254.
[31] R.F. Zhang, T.C. Germann, J. Wang, X.Y. Liu, I.J. Beyerlein, Role of interface structure on the plastic response of Cu/Nb nanolaminates under shock compression: non-equilibrium molecular dynamics simulations, Scripta Mater. 68 (2) (2013) 114–117.
[32] N. Gupta, M.I. Baskes, S.G. Srinivasan, The role of interface structure in spallation of a layered nanocomposite, JOM 63 (9) (2011) 74.
[33] L.F. Zeng, R. Gao, Q.F. Fang, X.P. Wang, Z.M. Xie, S. Miao, T. Hao, T. Zhang, High strength and thermal stability of bulk Cu/Ta nanolamellar multilayers fabricated by cross accumulative roll bonding, Acta Mater. 110 (Supplement C) (2016) 341–351.
[34] S. Plimpton, Fast parallel algorithms for short-range molecular dynamics, J. Comput. Phys. 117 (1) (1995) 1–19.
[35] G.P. Purja Pun, K.A. Darling, L.J. Kecskes, Y. Mishin, Angular-dependent interatomic potential for the Cu–Ta system and its application to structural stability of nano-crystalline alloys, Acta Mater. 100 (Supplement C) (2015) 377–391.
[36] C.L. Kelchner, S.J. Plimpton, J.C. Hamilton, Dislocation nucleation and defect structure during surface indentation, Phys. Rev. B. 58 (17) (1998) 11085–11088.
[37] J.D. Honeycutt, H.C. Andersen, Molecular dynamics study of melting and freezing of small Lennard-Jones clusters, J. Phys. Chem. 91 (19) (1987) 4950–4963.
[38] S. Alexander, V.B. Vasily, A. Athanasios, Automated identification and indexing of dislocations in crystal interfaces, Modell. Simul. Mater. Sci. Eng. 20 (8) (2012) 085007.
[39] S. Alexander, A. Karsten, Extracting dislocations and non-dislocation crystal defects from atomistic simulation data, Modell. Simul. Mater. Sci. Eng. 18 (8) (2010) 085001.
[40] A. Stukowski, Computational analysis methods in atomistic modeling of crystals, JOM 66 (3) (2014) 399–407.
[41] K. Mackenchery, R.R. Valisetty, R.R. Namburu, A. Stukowski, A.M. Rajendran, A.M. Dongare, Dislocation evolution and peak spall strengths in single crystal and nanocrystalline Cu, J. Appl. Phys. 119 (4) (2016) 044301.
[42] G. Agarwal, R.R. Valisetty, R.R. Namburu, A.M. Rajendran, A.M. Dongare, The quasi-coarse-grained dynamics method to unravel the mesoscale evolution of defects/damage during shock loading and spall failure of polycrystalline Al microstructures, Sci. Rep. 7 (1) (2017) 12376.
[43] J. Chen, M.A. Tschopp, A.M. Dongare, Role of nanoscale Cu/Ta interfaces on the shock compression and spall failure of nanocrystalline Cu/Ta systems at the atomic scales, J. Mater. Sci. (2017).
[44] G. Agarwal, A.M. Dongare, Shock wave propagation and spall failure in single crystal Mg at atomic scales, J. Appl. Phys. 119 (14) (2016) 145901.
[45] J. Chen, M.A. Tschopp, A.M. Dongare, Shock wave propagation and spall failure of nanocrystalline Cu/Ta alloys: effect of Ta in solid-solution, J. Appl. Phys. 122 (22) (2017) 225901.
[46] K.T. Ramesh, High Rates and Impact Experiments, in: W.N. Sharpe (Ed.), Springer Handbook of Experimental Solid Mechanics, Springer, US, Boston, MA, 2008, pp. 929–960.
[47] Z. Shi, C.V. Singh, Competing twinning mechanisms in body-centered cubic metallic nanowires, Scripta Mater. 113 (2016) 214–217.
[48] G. Sainath, B.K. Choudhary, Deformation behaviour of body centered cubic iron nanopillars containing coherent twin boundaries, Philos. Mag. 96 (32-34) (2016) 3502–3523.
[49] I.J. Beyerlein, J. Wang, R. Zhang, Mapping dislocation nucleation behavior from bimetal interfaces, Acta Mater. 61 (19) (2013) 7488–7499.
[50] L. Lu, C. Huang, W. Pi, H. Xiang, F. Gao, T. Fu, X. Peng, Molecular dynamics simulation of effects of interface imperfections and modulation periods on Cu/Ta multilayers, Comput. Mater. Sci. 143 (2018) 63–70.
[51] S. Shao, S.N. Medyanik, Interaction of dislocations with incoherent interfaces in nanoscale FCC–BCC metallic bi-layers, Modell. Simul. Mater. Sci. Eng. 18 (5) (2010) 055010.
[52] A. Hashibon, C. Elsässer, Y. Mishin, P. Gumbsch, First-principles study of thermodynamical and mechanical stabilities of thin copper film on tantalum, Phys. Rev. B. 76 (24) (2007) 245434.
[53] A.M. Dongare, A.M. Rajendran, B. LaMattina, M.A. Zikry, D.W. Brenner, Atomic scale simulations of ductile failure micromechanisms in nanocrystalline Cu at high strain rates, Phys. Rev. B. 80 (10) (2009) 104108.